ACS Catalysis

Letter

pubs.acs.org/acscatalysis

Activation of [$CrCl_3${R-SN(H)S-R}] Catalysts for Selective Trimerization of Ethene: A Freeze-Quench Cr K-Edge XAFS Study

Stuart A. Bartlett,[†,‡] Jerome Moulin,[†] Moniek Tromp,[§] Gillian Reid,[†] Andrew J. Dent,[⊥] Giannantonio Cibin,[⊥] David S. McGuinness,[∥] and John Evans*[,†,‡,⊥]

[†]Chemistry, University of Southampton, Highfield, Southampton, SO17 1BJ, United Kingdom

[‡]Research Complex at Harwell, Rutherford Appleton Laboratory, Didcot, OX11 0FA, United Kingdom

[§]Catalysis Research Center, Technische Universität München, Ernst-Otto-Fischer-Straße 1, 85748 Garching, Germany

[⊥]Diamond Light Source, Rutherford Appleton Laboratory, Didcot, OX11 0DE, United Kingdom

[∥]School of Physical Sciences - Chemistry, University of Tasmania, Hobart 7001, Australia

Supporting Information

ABSTRACT: Homogeneous chromium catalysts for the selective conversion of ethene to hex-1-ene are formed from Cr(III) reagents, aminothioether ligands of the type HN-$(CH_2CH_2SR)_2$, and aluminum reagents. In this study, the early activation steps are investigated by EPR, UV−visible, and Cr K-edge XAFS spectroscopy; rapid stopped-flow mixing and a freeze-quench allows good quality EXAFS analysis of a species formed in ∼1 s of reaction. This is shown to involve reduction to Cr(II) and deprotonation of a NH group of the auxiliary ligand. This 4-coordinate metal center may act as precursor for the coordination of ethene and subsequent selective oligomerization.

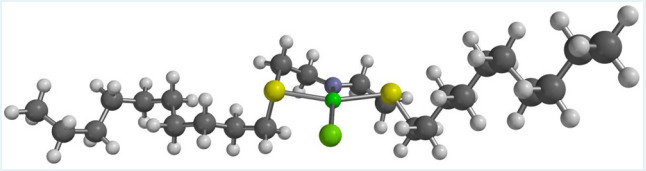

KEYWORDS: *homogeneous catalysis, chromium, oligomerization, XAFS spectroscopy, DFT calculations*

The selective trimerization of ethene to hex-1-ene catalyzed by chromium provides improved atom efficiency over chain-growth processes.[1,2] Highly effective catalysts for this trimerization have been reported from precursors of the type [$CrCl_3${R-SN(H)S-R}] **1** (R-SN(H)S-R = $HN(CH_2CH_2SR)_2$ with methylaluminoxane (MAO) as promoter.[3] Such activation of precursors has generally been investigated via the crystallization of reaction products. Reaction of **1** (R = Cy) with 10 $AlMe_3$ effected partial methylation to a Cr(III) product [$(\mu$-$Cl)_2${$CrMe$(R-SN(H)S-R)}$_2$][$AlMe_3Cl]_2$.[4] However, with *iso*-butylaluminoxane reduction to a Cr(II) relative, [$(\mu$-$Cl)_2${Cr(R-SN(H)S)-R}$_2$][$AlCl_2{}^iBu_2]_2$ was isolated instead, and the preferred oxidation state depends upon the alkylaluminum.[5] We have previously utilized Cr K-edge X-ray absorption spectroscopy to explore activation steps in solution.[6] However, these measurements required about 3−4 h of data, as has been recently reported for activation of $Cr(acac)_3$ with bidentate diphosphinoamine (PNP) ligands.[7] Low temperature reactions between $CrCl_3$(PNP) type complexes and MAO using EPR and UV−visible spectroscopy as probes have also been recently reported, with Cr(III) species observed at low temperatures.[8] In this work, we combine stopped-flow mixing and a freeze-quench technique by which the reaction can be frozen within ∼1 s of mixing.[9,10] The prospective roles of MAO, generally employed in high excess, have been replaced by near stoichiometric quantities of the well-defined $AlMe_3$ as the alkyl source and [Ph_3C][$Al\{OC(^tBu^F)_3\}_4$] to provide a Lewis acid with a weakly coordinating counterion. By interrogating the solution after rapid mixing, we have identified a new Cr(II) intermediate, which may be formed en route to the entry point of the catalytic reaction.

Addition of $AlMe_3$ to **1** (R = *n*-decyl) in a toluene/CH_2Cl_2 solution caused rapid changes in the EPR signal when recorded as a frozen glass with the signal of **1** being lost upon addition of $3AlMe_3$/1Cr (Figure S1, Supporting Information (SI)). Stopped-flow UV−visible spectroscopy (SI Figure S2) displayed a change faster than 1 s, followed by a further gradual change over a total reaction time of ∼30 s.

Comparisons of the XANES and Fourier transforms of the Cr K-edge EXAFS of **1** (R = *n*-decyl) in toluene (5 mM) and four reactions are presented in Figure 1; the reactions performed at room temperature are compared with the stopped-flow freeze-quench reaction with 20 equiv of $AlMe_3$ reaction, quenched after 1 s reaction time (the reaction of **1** with 10 equiv of $AlMe_3$ freeze-quenched after 300 s, and 10 equiv of $AlMe_3$ quenched after 1 s displayed similar spectra). The XANES and EXAFS spectra show that there is a rapid reaction between **1** and $AlMe_3$ to form a new species **2** (R = *n*-decyl). Extending the reaction time at room temperature resulted in the observation of a different product, **3**, but the presence of the Lewis acid [Ph_3C][$Al\{OC(^tBu^F)_3\}_4$], **4**, appeared to stabilize product **2**. The raw EXAFS data and fits for **1**, **2** (Figure 2), the room temperature reaction of **1** with $AlMe_3$ forming product **3**, and the reaction of **1** with LiMe (4

Received: July 16, 2014
Revised: October 16, 2014
Published: October 21, 2014

   dx.doi.org/10.1021/cs501017g | *ACS Catal.* 2014, 4, 4201−4204

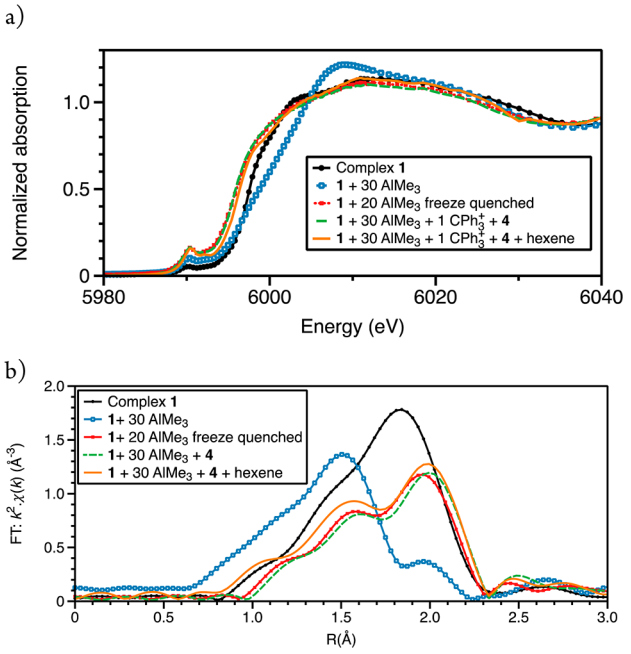

Figure 1. At the Cr K-edge: (a) XANES and (b) Fourier transforms of k^2-weighted EXAFS data for $[CrCl_3\{R\text{-}SN(H)S\text{-}R\}]$ **1** (R = decyl) (•) (5 mM in toluene) and reactions with $AlMe_3$.

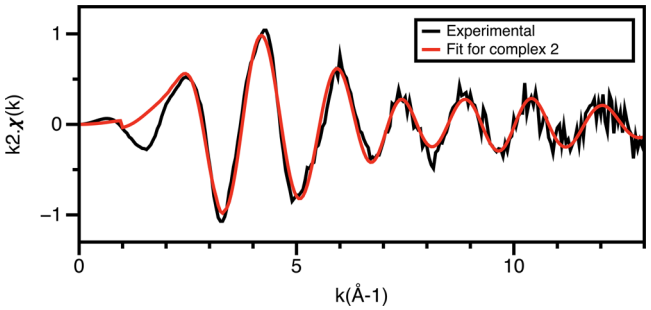

Figure 2. Cr K-edge k^2-weighted EXAFS data for $[CrCl_3\{R\text{-}SN(H)S\text{-}R\}]$ **1** (R = decyl) and $AlMe_3$ in toluene, freeze-quenched.

equiv) are given in SI Figures S3–S6 and Tables S1–S4. The structural parameters derived from the EXAFS analyses are summarized in Table 1. Reaction with MeLi appears to cause loss of all Cr–S and Cr–Cl within the coordination shell.

Product **3** displays a predominance of light atoms in the coordination shell with the loss of the chloride from complex **1** (R = *n*-decyl) (Table 1). In contrast, analysis of the 1 s freeze-quenched $AlMe_3$ reaction indicated retention of the R-SNS ligand and a reduced coordination number (1) of the Cr–Cl forming a coordination sphere of [CrCl(S–N–S)] **2**. Also apparent is a small shift to lower energy for the absorption edge features (Figure 1a). Substitution of chloride by methyl at the chromium is expected to be accompanied by a shift in the absorption edge feature to higher energy.[11]

Table 1. Structural Parameters from Cr K-Edge EXAFS Analysis for $[CrCl_3\{R\text{-}SN(H)S\text{-}R\}]$ 1 (R = *n*-decyl) (5 mM in toluene) and Reactions with Excess $AlMe_3$[a]

species	coordination shell	*d*(Cr–X) (Å)
	1 Cr–N	2.07(4)
1	3 Cr–Cl	2.32
	2 Cr–S	2.45
2	1.4(3) Cr–N	2.02(2)
	1 Cr–Cl	2.32(3)
	2 Cr–S	2.46(2)
3	3.6(6) Cr–C/N	1.97(1)
	2.1(2) S/Cl	2.31(3)

[a]Parameters without standard deviations were optimized manually.

XANES simulations using FEFF9[12] were performed on potential structures, starting from **1** (R = *n*-Bu).[3] Stepwise substitution of chloride by methyl indeed did lead to a shift of the edge features to higher energy (Figure 3). The low

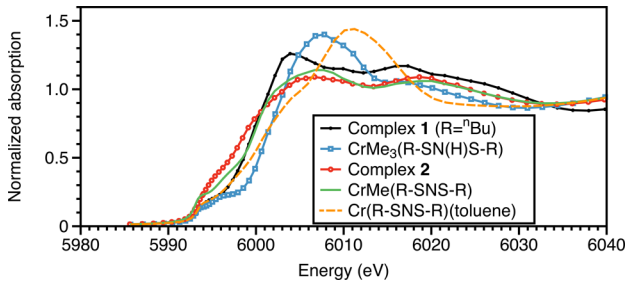

Figure 3. Calculations of the Cr K-edge XANES for **1** (R = ^{n}Bu) and possible reaction products.

coordination numbers from the EXAFS analysis of product **2** and the reaction of **1** with $AlMe_3$ frozen after 1 s suggest a species similar to $[Cr(Cl\text{–}AlEtCl_2)\{R\text{-}SN(H)S\text{-}R\}]AlEtCl_3$.[5] Using the structure of this, the shift in the absorption edge to lower energy was indeed observed in simulations; the methylated version $[Cr(CH_3)\{R\text{-}SN(H)S\text{-}R\}]^+$ showed again an upward shift in absorption edge energy. An edge position analysis,[10] (SI Table S5) reconfirmed that the edge shapes and position not only are dependent on oxidation state, but also are sensitive to the type, number, and relative position of the neighboring atoms. A changed coordination from the distorted octahedral **1** to a square planar structure **2** (Cr^{II}) did reproduce the experimentally observed shift of the edge features.

A species of the type [CrCl(S–N–S)] could exist as Cr(II) or Cr(I) in high, intermediate, or low spin states; it may also possess a N-deprotonated $(R\text{-}SNS\text{-}R)^-$ ligand, as demonstrated to occur on treatment of **1** with $AlMe_3$.[13] The absence of N-deprotonation has been previously proposed in a theoretical study of the catalytic cycle of ethene trimerization,[14] but this work did not consider pathways for forming the catalytic species. These options were compared by a broad structural survey using DFT calculations with R = Me. The Cr-to-ligand bond lengths for a series of options for **2** in different spin states are given in SI Table S6. The high spin state (S = 2) was found to be much more stable than either the intermediate (S = 1) or low (S = 0) spin state (by 44 and 50 kcal/mol, respectively). The favorability of the S = 2 state over S = 0 was reduced as Cl was replaced by Me, toluene, and ethene (to 41, 38, and 12 kcal/mol, respectively).

A potential route for the formation of **2** (Scheme 1) via initial NH deprotonation and Cl^- ligand loss to form $[CrCl_2(R\text{-}SNS)]$ ($\Delta G°$ −7.5 kcal/mol) is similar to the observations on the reaction of $[ScCl_3\{R\text{-}SN(H)S\text{-}R\}]$ with LiMe.[10] Following methylation to [CrClMe(R-SNS-R)] {$\Delta G°$ −30.0 kcal/mol relative to **1** (R = Me) and Al_2Me_6}, a reductive elimination of ethane, as is known for Cr(III),[15] can form **2** ($\Delta G°$ −44.8 kcal/mol vs **1**), possibly by a dinuclear process[16] rather than loss of a methyl radical.

dx.doi.org/10.1021/cs501017g | ACS Catal. 2014, 4, 4201–4204

Scheme 1. Proposed Steps To Form Complex 2

$[CrCl_3\{R\text{-}SN(H)S\}] + \frac{1}{2}Al_2Me_6 = [CrCl_2\{R\text{-}SNS\text{-}R\}] + \frac{1}{2}Al_2Me_4Cl_2 + CH_4$

$[CrCl_2\{R\text{-}SNS\text{-}R\}] + \frac{1}{2}Al_2Me_6 = [CrClMe\{R\text{-}SNS\text{-}R\}] + \frac{1}{2}Al_2Me_4Cl_2$

$[CrClMe\{R\text{-}SNS\text{-}R\}] = [CrCl\{R\text{-}SNS\text{-}R\}Cl] + \frac{1}{2}C_2H_6$

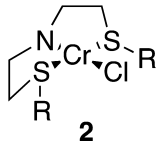

2

High spin states were significantly favored, and reaction steps from the reagents **1** and $AlMe_3$ to $[Cr^{II}Cl\{R\text{-}SNS\text{-}R\}]$ (S = 2) **2** provided the lowest-energy product (e.g., $\Delta G°$ −40 and −31 kcal/mol relative to $[Cr^{II}Cl\{R\text{-}SN(H)S\text{-}R\}]^+$ and $[Cr^{I}Cl\{R\text{-}SN(H)S\text{-}R\}]$, respectively) (Figure 4). The minimized

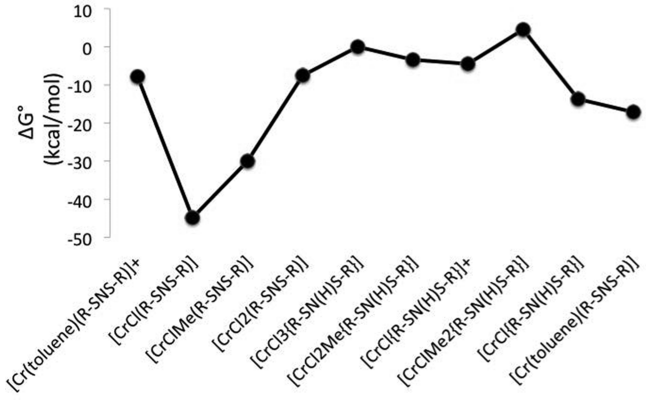

Figure 4. Calculated $\Delta G°$ (kcal/mol) of reaction steps from $[CrCl_3\{R\text{-}SN(H)S\text{-}R\}]$ **1** (R = Me) per Cr atom relative to **1**, Al_2Me_6, and toluene.

structure of the square planar geometry of **2** with a planar amido ligand in this spin state afforded bond distances close to those obtained from the EXAFS analysis (Cr−N, 1.98; Cr−Cl, 2.35; Cr−S, 2.47 Å). The Cr-to-ligand distances are generally sensitive to the spin multiplicity (SI Table S6), with bond lengths of 1.85 and 2.08 (Cr−N), 2.32 and 2.25 (Cr−Cl), and 2.36 and 2.36 (Cr−S) Å calculated for S = 0 and S = 1 $[Cr^{II}Cl\{R\text{-}SNS\text{-}R\}]$, respectively. Nine different theoretical models were used to check the proposal of structure **2** (SI Table S7). The Cr−Cl and mean Cr−S distances for **2** (R = Me and *n*-decyl) were all within the experimental error of the EXAFS analysis, and the span of the Cr−N distances (1.97−1.99 Å for R = Me and 1.98−2.00 for R = *n*-decyl) was close to the experimental value for R = *n*-decyl (2.02(2) Å). The calculated (TDDFT) UV−visible spectrum of **2** (S = 2) shows shifts in both the main bands in this region that follow the experimentally observed trend (from 664 and 467 nm in **1** to 589 and 389 nm in **2**) (SI Figure S7).

Figure 4 also includes further reactions to toluene solvates. The most stable structure located, of toluene complexes of the type $[Cr(R\text{-}SNS\text{-}R)(toluene)]^{n+}$ (*n* = 0,1), was high spin for Cr(II), in which the toluene adopted an η^2-coordination mode (**5a**). The favored Cr(I) state, (S = 3/2), also displayed a modified coordination of the arene, with some 1,4-coordination character, as well as one greatly extended Cr−S bond (3.81 Å) (**5b**) (Scheme 2). Although DFT calculations showed that these toluene complexes could act as precursors to the ethene

Scheme 2. Favorable Structures Calculated for $[Cr(R\text{-}SNS\text{-}R)(toluene)]^{n+}$ for Cr(II) (S = 2) 5a and Cr(I) (S = 3/2) 5b

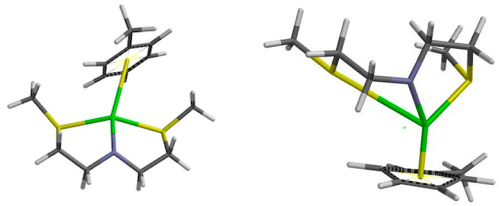

5a **5b**

trimerization cycle after ethene substitution, they were not observed in this study. Formation of these complexes from **2** appears unlikely (Figure 4) without addition of a stronger Lewis acid.

The increase in energy of the absorption edge feature observed for the room temperature solution (Figure 1a), species **3**, could occur by substitution of chloride for a carbon donor either by alkylation or arene coordination (Figure 3). From the Cr(II) complex **2**, disproportionation (eq 1) was calculated to be unfavorable (C_7H_8 = toluene):

$$2[CrCl\{R\text{−}SNS\text{−}R\}] + C_7H_8 = [Cr\{R\text{−}SNS\text{−}R\}(C_7H_8)] + [CrCl_2\{R\text{−}SNS\text{−}R\}] \quad (1)$$

Further substitution of the $(R\text{-}SNS\text{-}R)^-$ ligand to form $[Cr(C_7H_8)_2]^+$ was also found to be extremely unfavorable. This is consistent with the literature report that the reoxidation of $[Cr(Cl\text{−}AlEtCl_2)\{R\text{-}SN(H)S\text{-}R\}]AlEtCl_3$ is accompanied by precipitation of Cr metal, rather than a Cr^I/Cr^{III} couple.[5] Indeed, a dark precipitate was observed after the recording of the XAFS spectrum of **3** at room temperature. It appears that complex **2** decomposes by disproportionation to metallic chromium and a Cr(III) species **3** in solution. The near edge spectrum of **3** (Figure 1a) exhibits a shift to higher energy, as observed by XANES simulations for $[CrMe_3\{R\text{-}SN(H)\text{-}R\}]$ (Figure 3). Given that complex **2** is considered to contain a deprotonated ligand, and that the EXAFS analysis provides a coordination number for the Cr−C/N shell between three and four, the evidence favors $[CrMe_2(R\text{-}SNS\text{-}R)]$ as an average formulation of **3**; DFT calculations on a variety of options indicate shorter Cr−N and Cr−S distances of coordination sites such as **3**, as compared with 6-coordinate centers (SI Table S8).

The results indicate that the trimerization catalyst precursor **1** undergoes a rapid ligand N-deprotonation, a lowering of the coordination number, and reduction to Cr(II), to form the 4-coordinate species **2**. This differs from the self-activating pyridine−SNS complexes of Gambarotta et al.,[17] and this may, in part, be due to the presence of the N−H group affording an anionic amido ligand, facilitating halide dissociation. Although it is evident that the EXAFS analysis would fail to identify any hydride ligand within **2**, the change in electronic properties and coordination geometry of the chromium will affect the XANES features. FEFF calculations showed that incorporation of hydrides would cause a shift of the edge features to higher energy (SI Figure S9), unlike the observed spectrum (Figure 1a). An alternative stabilization could be via agostic interactions

dx.doi.org/10.1021/cs501017g | ACS Catal. 2014, 4, 4201−4204

of the *n*-decyl side chains to the chromium atom. Some evidence for a weak interaction of this nature was apparent in the DFT calculations using the ωB97X-D functional (designed to model long-range interactions). One Cr···H−C distance to one of the S−CH_2 sites was reduced from a normal closest approach of ∼3.3 Å to ∼3.0 Å.

Cr(I) complexes with η^6-arenes have been shown to afford trimerization catalysts.[18] The inclusion of Lewis acids can assist a route to η^2-arene complexes opening a clear path to alkene coordination and a trimerization cycle.[19] Evidently, the inclusion of $[Ph_3C][Al\{OC(^tBu^F)_3\}_4]$ **4** stabilized **2**, but did not lead to the formation of the arene complexes under these mild conditions. Ethene trimerization cycles starting from the arene complexes **5a** (R = Me) and **5b** (R = Me) were both modeled by DFT calculations (SI Figure S10). For the Cr(I/III) cycle, the initial displacement of toluene by ethene was strongly exergonic (Δ*G*° −29 kcal/mol), indicating that under the more forcing conditions and with the Lewis acid sites in MAO promoters, a route from **2** to the catalytic cycles is plausible.

Identification of the Cr(II) species **2** by freeze-quench procedures has provided new insight into the genesis of the catalytic cycle; conventional XAFS observation would have detected only the Cr(III) "decomposition" product, **3**.

■ ASSOCIATED CONTENT

Supporting Information

Experimental details, XAFS, UV−visible, EPR spectra, DFT calculations. This material is available free of charge via the Internet at http://pubs.acs.org.

■ AUTHOR INFORMATION

Corresponding Author

* E-mail: je@soton.ac.uk, john.evans@diamond.ac.uk.

Notes

The authors declare no competing financial interest.

■ ACKNOWLEDGMENTS

We wish to thank EPSRC for funding this project (EP/032463/1 and EP/I01974X/1), Diamond Light Source Ltd and the ESRF for access to the synchrotron facilities and staff at B18 and BM26A for their assistance. We also thank Prof. R. P. Tooze and Dr. M. Hanton (Sasol Technology UK) for helpful discussions.

■ REFERENCES

(1) Reagen, W. K. Patent EP 0417477 B1, 1995.

(2) McGuinness, D. S. *Chem. Rev.* **2011**, *111*, 2321−2341. Agapie, T. *Coord. Chem. Rev.* **2011**, *255*, 861−880. Wass, D. F. *Dalton Trans.* **2007**, 816−819. Dixon, J. T.; Green, M. J.; Hess, F. M.; Morgan, D. H. *J. Organomet. Chem.* **2004**, *689*, 3641−3668.

(3) McGuinness, D. S.; Wasserscheid, P.; Keim, W.; Dixon, J. T.; Bollmann, A.; Maumela, H.; Hess, F.; Englert, U. *J. Am. Chem. Soc.* **2003**, *125*, 5272−5273.

(4) Jabri, A.; Temple, C.; Crewdson, P.; Gambarotta, S.; Korobkov, I.; Duchateau, R. *J. Am. Chem. Soc.* **2006**, *128*, 9238−9247.

(5) Temple, C.; Jabri, A.; Crewdson, P.; Gambarotta, S.; Korobkov, I.; Duchateau, R. *Angew. Chem., Int. Ed.* **2006**, *45*, 7050−7053.

(6) Moulin, J. O.; Evans, J.; McGuinness, D. S.; Reid, G.; Rucklidge, A. J.; Tooze, R. P.; Tromp, M. *Dalton Trans.* **2008**, 1177−1185.

(7) Rabeah, J.; Bauer, M.; Baumann, W.; McConnell, A. E. C.; Gabrielli, W. F.; Webb, P. B.; Selent, D.; Brückner, A. *ACS Catal.* **2013**, *3*, 95−102.

(8) Do, L. H.; Labinger, J. A.; Bercaw, J. E. *ACS Catal.* **2013**, *3*, 2582−2585.

(9) Bartlett, S. A.; Wells, P. P.; Nachtegaal, M.; Dent, A. J.; Cibin, G.; Reid, G.; Evans, J.; Tromp, M. *J. Catal.* **2011**, *284*, 247−248.

(10) Bartlett, S. A.; Cibin, G.; Dent, A. J.; Evans, J.; Hanton, M. J.; Reid, G.; Tooze, R. P.; Tromp, M. *Dalton Trans.* **2013**, *42*, 2213−2223.

(11) Tromp, M.; Moulin, J.; Reid, G.; Evans, J. *AIP Conf. Proc.* **2007**, *882*, 699−701.

(12) Rehr, J. J.; Kas, J. J.; Prange, M. P.; Sorini, A. P.; Takimoto, Y.; Vila, F. *C. R. Phys.* **2009**, *10*, 548−559. Rehr, J. J.; Kas, J. J.; Vila, F. D.; Prange, M. P.; Jorissen, K. *Phys. Chem. Chem. Phys.* **2010**, *12*, 5503−5513.

(13) McGuinness, D. S.; Brown, D. B.; Tooze, R. P.; Hess, F. M.; Dixon, J. T.; Slawin, A. M. Z. *Organometallics* **2006**, *25*, 3605−3610.

(14) Yang, Y.; Liu, Z.; Qiu, P.; Dong, Q.; Vanderbilt, J.; Liu, B. *Organometallics* **2011**, *30*, 5297−5302.

(15) Heintz, R. A.; Leelasubcharoen, S.; Liable-Sands, L. M.; Rheingold, A. L.; Theopold, K. H. *Organometallics* **1998**, *17*, 5477−5485.

(16) Evans, J.; Norton, J. R. *J. Am. Chem. Soc.* **1974**, *96*, 7577−7578. Norton, J. R. *Acc. Chem. Res.* **1979**, *12*, 139−145.

(17) Albahily, K.; Shaikh, Y.; Ahmed, Z.; Korobkov, I.; Gambarotta, S.; Duchateau, R. *Organometallics* **2011**, *30*, 4159−4164.

(18) Jabri, A.; Mason, C. B.; Sim, Y.; Gambarotta, S.; Burchall, T. J.; Duchateau, R. *Angew. Chem., Int. Ed.* **2008**, *47*, 9717−9721.

(19) Overett, M. J.; Blaan, K.; Bollmann, A.; Dixon, J. T.; Haasbroek, D.; Killian, E.; Maumela, H.; McGuinness, D. S.; Morgan, D. H. *J. Am. Chem. Soc.* **2005**, *127*, 10723−10730.